Mineralogical Magazine (2023), **87**, 204–217
doi:10.1180/mgm.2022.129

CAMBRIDGE UNIVERSITY PRESS

Article

Piccoliite, $NaCaMn_2^{3+}(AsO_4)_2O(OH)$, a new arsenate from the manganese deposits of Montaldo di Mondovì and Valletta, Piedmont, Italy

Fernando Cámara[1*], Cristian Biagioni[2], Marco E. Ciriotti[3,4], Ferdinando Bosi[5,6], Uwe Kolitsch[7,8], Werner H. Paar[9], Ulf Hålenius[10], Giovanni O. Lepore[11], Günter Blass[12] and Erica Bittarello[13]

[1]Dipartimento di Scienze della Terra Ardito "Ardito Desio", Università degli Studi di Milano, via Luigi Mangiagalli 34, I-20133 Milano, Italy; [2]Dipartimento di Scienze della Terra, Università di Pisa, via Santa Maria 53, I-56126 Pisa, Italy; [3]Associazione Micromineralogica Italiana, via San Pietro 55, I-10073 Devesi-Cirié, Italy; [4]Dipartimento di Scienze della Terra, Università degli Studi di Torino, via Tommaso Valperga Caluso 35, 10125 Torino, Italy; [5]Dipartimento di Scienze della Terra, Sapienza Università di Roma, piazzale Aldo Moro 5, I-00185 Roma, Italy; [6]CNR, Istituto di Geologia Ambientale e Geoingegneria, U.O.S. di Roma, Roma, Italy; [7]Mineralogisch-Petrographische Abt., Naturhistorisches Museum, Burgring 7, A-1010 Wien, Austria; [8]Institut für Mineralogie und Kristallographie, Universität Wien, Josef-Holaubek-Platz 2, A-1090 Wien, Austria; [9]Consultant, Department of Materials Science and Physics, University of Salzburg, Jakob-Haringer-Strasse 2a, 5020 Salzburg, Austria; [10]Department of Geosciences, Swedish Museum of Natural History, Box 50007, SE-10405 Stockholm, Sweden; [11]Dipartimento di Scienze della Terra, Università degli Studi di Firenze, via La Pira 4, I-50121 Florence, Italy; [12]Independent Researcher, Merzbachstraße 6, D-52249 Eschweiler, Germany; and [13]SpectraLab s.r.l. - Spin-off accademico dell'Università degli Studi di Torino, via Tommaso Valperga Caluso 35, 10125 Torino, Italy

Abstract

Piccoliite, ideally $NaCaMn_2^{3+}(AsO_4)_2O(OH)$, is a new mineral discovered in the Fe–Mn ore hosted in metaquartzites of the Montaldo di Mondovì mine, Corsaglia Valley, Cuneo Province, Piedmont, Italy. It occurs as small and rare black crystals and aggregates hosted by a matrix of quartz, associated with calcite and berzeliite/manganberzeliite. It has been also found in the Valletta mine near Canosio, Maira Valley, Cuneo Province, Piedmont, Italy, where it occurs embedded in quartz associated with grandaite, hematite, tilasite/adelite and rarely thorianite. The mineral is opaque (thin splinters may be very dark red), with brown streak and has a resinous to vitreous lustre. It is brittle with irregular fracture. No cleavage has been observed. The measured Mohs hardness is ~5–5.5. Piccoliite is non fluorescent. The calculated density is 4.08 g·cm^{-3}. Chemical spot analyses by electron microprobe analysis using wavelength dispersive spectroscopy resulted in the empirical formula (based on 10 anions per formula unit) $(Na_{0.64}Ca_{0.35})_{\Sigma 0.99}(Ca_{0.75}Na_{0.24})_{\Sigma 0.99}(Mn^{3+}_{1.08}Fe^{3+}_{0.59}Mg_{0.20}Ca_{0.10})_{\Sigma 1.97}(As_{2.03}V_{0.03}Si_{0.01})_{\Sigma 2.07}O_9(OH)$ and $(Na_{0.53}Ca_{0.47})_{\Sigma 1.00}(Ca_{0.76}Na_{0.23}Sr_{0.01})_{\Sigma 1.00}(Mn^{3+}_{0.63}Fe^{3+}_{0.49}Mg_{0.48}Mn^{4+}_{0.34}Ca_{0.06})_{\Sigma 2.00}(As_{1.97}P_{0.01}Si_{0.01})_{\Sigma 1.99}O_9(OH)$ for the Montaldo di Mondovì and Valletta samples, respectively. The mineral is orthorhombic, *Pbcm*, with single-crystal unit-cell parameters $a = 8.8761(9)$, $b = 7.5190(8)$, $c = 11.689(1)$ Å and $V = 780.1(1)$ Å^3 (Montaldo di Mondovì sample) and $a = 8.8889(2)$, $b = 7.5269(1)$, $c = 11.6795(2)$ Å, $V = 781.43(2)$ Å^3 (Valletta sample) with $Z = 4$. The seven strongest powder X-ray diffraction lines for the sample from Montaldo di Mondovì are [*d* Å (I_{rel}; *hkl*)]: 4.85 (57; 102), 3.470 (59; 120, 113), 3.167 (100; 022), 2.742 (30; 310, 213), 2.683 (53; 311, 023), 2.580 (50; 222, 114) and 2.325 (19; 320, 214, 223). The crystal structure ($R_1 = 0.0250$ for 1554 unique reflections for the Montaldo di Mondovì sample and 0.0260 for 3242 unique reflections for the Valletta sample) has $MnO_5(OH)$ octahedra forming edge-shared dimers; these dimers are connected through corner-sharing, forming two-up-two-down $[^{[6]}M_2(^{[4]}TO_4)_4\varphi_2]$ chains [M = Mn; T = As; φ = O(OH)] running along [001]. These chains are bonded in the **a** and **b** directions by sharing corners with AsO_4 tetrahedra, giving rise to a framework of tetrahedra and octahedra hosting seven-coordinated Ca^{2+} and Na^+ cations. The crystal structure of piccoliite is closely related to that of pilawite-(Y) as well as to carminite-group minerals that also show the same type of chains but with different linkage. The mineral is named after the mineral collectors Gian Paolo Piccoli and Gian Carlo Piccoli (father and son) (1926–1996 and b. 1953, respectively), the latter having discovered the type material at the Montaldo di Mondovì mine.

Keywords: piccoliite, new-mineral, manganese arsenate, crystal structure, Raman, Montaldo mine, Piedmont, Italy

(Received 23 September 2022; accepted 11 November 2022; Accepted Manuscript published online: 28 November 2022; Associate Editor: Daniel Atencio)

Introduction

The north of Italy is rather rich in manganese deposits. Among the 391 species described so far in Italy, 16 species contain Mn^{3+} and all of them are from a Ligurian or Piedmontese (*s.l.*) manganese type-locality deposit (Table 1). Piccoliite, $NaCaMn_2^{3+}(AsO_4)_2O(OH)$, was first recognised on a specimen found in 2007 by Gian

***Author for correspondence:** Fernando Cámara, Email: fernando.camara@unimi.it
Cite this article: Cámara F., Biagioni C., Ciriotti M.E., Bosi F., Kolitsch U., Paar W.H., Hålenius U., Lepore G.O., Blass G. and Bittarello E. (2023) Piccoliite, $NaCaMn_2^{3+}(AsO_4)_2O(OH)$, a new arsenate from the manganese deposits of Montaldo di Mondovì and Valletta, Piedmont, Italy. *Mineralogical Magazine* **87**, 204–217. https://doi.org/10.1180/mgm.2022.129

Table 1. Italian type minerals containing essential Mn^{3+}.

Mineral species	Formula	Reference
Alpeite *	$Ca_4Mn^{3+}_2Al_2(Mn^{3+}Mg)(SiO_4)_2(Si_3O_{10})(V^{5+}O_4)(OH)_6$	1
Aldomarinoite #	$Sr_2Mn^{3+}(AsO_4)_2(OH)$	2
Braunite #	$Mn^{2+}Mn^{3+}_6(SiO_4)O_8$	3
Cerchiaraite-(Mn) *	$Ba_4Mn^{3+}_4O_3(OH)_3(Si_4O_{12})[Si_2O_3(OH)_4]Cl$	4
Coralloite *	$Mn^{2+}(H_2O)_4[Mn^{3+}_2(OH)_2(AsO_4)_2]$	5
Demagistrisite *	$(BaCa_2)Mn^{3+}_4[Si_3O_{10}][Si_2O_7](OH)_4{\cdot}3H_2O$	6
Lavoisierite #	$Mn^{2+}_8[Al_{10}(Mn^{3+}Mg)](PO_4)(SiO_4)_4(Si_2O_7)_2(Si_3O_{10})(OH)$	7
Lombardoite #	$Ba_2Mn^{3+}(AsO_4)_2(OH)$	2
Manganiakasakaite-(La) #	$(CaLa)(Mn^{3+}AlMn^{2+})(Si_2O_7)(SiO_4)O(OH)$	8
Manganiandrosite-(Ce) #	$(Mn^{2+}Ce)(Mn^{3+}AlMn^{2+})(Si_2O_7)(SiO_4)O(OH)$	9
Manganiceladonite *	$K(MgMn^{3+}\square)Si_4O_{10}(OH)_2$	10
Mozartite *	$CaMn^{3+}(SiO_4)(OH)$	11
Piccoliite #	$CaNaMn^{3+}_2(AsO_4)_2O(OH)$	12
Piemontite #	$(CaCa)(AlAlMn^{3+})(Si_2O_7)(SiO_4)O(OH)$	13
Piemontite-(Sr) *	$(CaSr)(AlAlMn^{3+})(Si_2O_7)(SiO_4)O(OH)$	14
Strontiomelane #	$Sr[Mn^{4+}_6Mn^{3+}_2]O_{16}$	15

* Liguria type localities; # Piedmont (and Aosta Valley) type localities.
References: 1 Kampf *et al.* (2017); 2 Cámara *et al.* (2022); 3 Haidinger (1828); 4 Basso *et al.* (2000); 5 Callegari *et al.* (2012); 6 Cámara *et al.* (2021b); 7 Orlandi *et al.* (2013); 8 Biagioni (2019); 9 Cenki-Tok *et al.* (2006); 10 Lepore *et al.* (2017); 11 Basso *et al.* (1993); 12 This work; 13 Kenngott (1853); 14 Bonazzi *et al.* (1990); 15 Meisser *et al.* (1999).

Carlo Piccoli in the dumps of the Montaldo di Mondovì mine (44°19'08.9"N, 7°51.09'5"E), Borgata Oberti, Montaldo di Mondovì, Corsaglia Valley, Piedmont, Italy (Fig. 1). A preliminary characterisation of the crystal structure of the mineral was provided by Kolitsch (2008). A second occurrence, which helped to improve the understanding of the mineral's crystal chemistry, was recognised in 2015 on specimens from the dumps of the Valletta mine (44°23'42"N, 7°5'42"E, 2536 m above sea level), Canosio, Maira Valley, Piedmont, Italy.

The name of the new mineral honours the mineral collectors Gian Carlo Piccoli (b. 1953) and his father Gian Paolo Piccoli (1928–1996) for their contribution to the knowledge of the regional mineralogy of Piedmont and Aosta Valley. Since the 1970s, father and son carried out mineralogical research in the Western Alps (Maritime and Cottian Alps, in the province of Cuneo, Piedmont), leading to the discovery of gramaccioliite-(Y) (Orlandi *et al.*, 2004) and grandaite (Cámara *et al.*, 2014), and to the creation of the mineralogical collection of the province of Cuneo, kept in the 'Federico Eusebio' civic museum in Alba, Cuneo Province, Piedmont. After his father's death, Gian Carlo Piccoli devoted himself to the writing of the books "*Minerali delle Alpi Marittime e Cozie – Provincia di Cuneo*" (Piccoli, 2002) and "*Minerali del Piemonte e della Valle d'Aosta*" (Piccoli *et al.*, 2007b). In this latter work, more than 570 different mineral species found in Piedmont and Aosta Valley are described. Finally, Gian Carlo Piccoli is co-author of the book "*Minerali in Val d'Ala*" (Maletto and Piccoli, 2014).

The mineral and its name (symbol Pcc) were approved by the Commission on New Minerals, Nomenclature and Classification of the International Mineralogical Association. (IMA2017-016, Cámara *et al.*, 2017). Cotype material from Montaldo di Mondovì is deposited in the Mineralogical Collection of the Museo di Storia Naturale, Università di Pisa, Via Roma 79, Calci, Pisa, Italy, under catalogue number 19906 and in the mineralogical collection of the Museo civico archeologico e di scienze naturali "Federico Eusebio" di Alba, Cuneo, Italy, with catalogue numbers M00673 (Montaldo di Mondovì specimen) and M00674 (Valletta specimen).

Fig. 1. Manganese ore cropping out along the Corsaglia river (Montaldo di Mondovì mine). In the photo is mineral collector Pierluigi Ambrino. Photo Marco E. Ciriotti, August 2014.

Occurrence

The Fe–Mn ores of the Montaldo di Mondovì mine were exploited for iron (Sismonda, 1841a, 1841b; Conti, 1873) from 1838 until its closure in the mid-1950s. The deposit is hosted within the 'Klippen of Deviglia' Unit (Vanossi, 1980) belonging to the Mesozoic sequence of the innermost Briançonnais Zone (Dalla Giovanna and Vanossi, 1991; Vanossi *et al.*, 1986). Metaquartzites and quartz-bearing marbles host the Fe–Mn ores that occur as layers, boudins, and, subordinately, in mineralised veins. Late-stage hematite-bearing veinlets crosscut both quartz arenites and marbles (Cabella *et al.*, 1992, 1995, 1999). The mineralisation consists of hollandite-supergroup minerals ± hematite ± braunite, with variable amounts of quartz, calcite, Mn- and Fe-rich muscovite and aegirine (Cabella *et al.*, 1999; Kolitsch *et al.*, 2011; Giai, 2020). Further details on the geological setting are reported in Cámara *et al.* (2021a) and references therein, which describe armellinoite-(Ce), $Ca_4Ce^{4+}(AsO_4)_4{\cdot}H_2O$, another arsenate for which the Montaldo di Mondovì mine is also the type locality. Other associated minerals include aegirine,

https://doi.org/10.1180/mgm.2022.129 Published online by Cambridge University Press

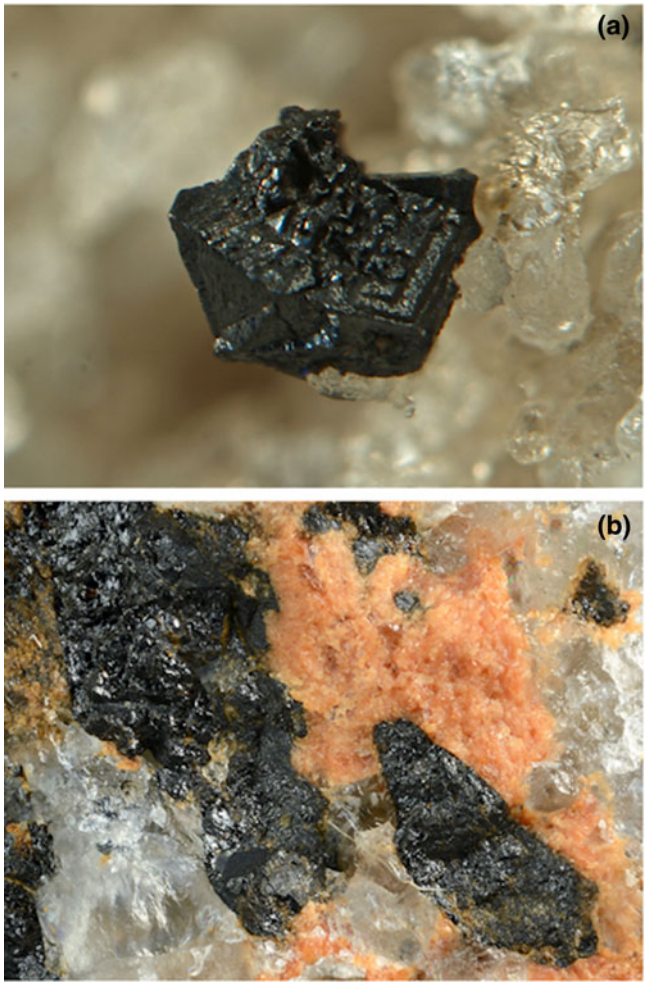

Fig. 2. Piccoliite from the two Italian occurrences. (a) A well-developed black crystal (1 mm) on quartz from the dump of the Montaldo di Mondovì mine. Collection Gianluca Armellino, photo Pierluigi Ambrino. (b) Black crystals of piccoliite associated with grandaite from the Valletta mine dump. Field of view 5 mm. Collection and photo Roberto Bracco.

anatase, armellinoite-(Ce), arsenogoyazite, berzeliite/manganberzeliite, braunite, calcite, chernovite-(Y), dolomite, cinnabar, cryptomelane, As-rich fluorapatite, gasparite-(Ce), gasparite-(La), goethite, hausmannite(?), hematite, hollandite, monazite-(Ce), montmorillonite, muscovite, orthoclase, pyrolusite(?), quartz, ramsdellite, ranciéite, romanèchite, rutile, spessartine, svabite, talmessite, tilasite, titanite wakefieldite-(Ce), wakefieldite-(Y), zircon, and three potential new minerals, i.e. the unnamed La-, Nd- and (Ca,Y,*REE*)-dominant analogues of chernovite-(Y) (Piccoli, 2002, 2007; Piccoli *et al.*, 2007a, 2007b; Ciriotti, 2007; Kolitsch *et al.*, 2011; Giai, 2020). Piccoliite at this locality always occurs in quartz–calcite veins (Fig. 2a), associated with calcite, berzeliite/manganberzeliite and, very rarely, with chernovite and the aforementioned unnamed rare earth element (REE) analogues of chernovite-(Y).

The Valletta mine was mined for iron in the 15th Century and probably hastily abandoned both due the uneconomic mixture of hematite with manganese ores and because it is located at a very high altitude (2536 m above sea level). The Fe–Mn deposit is located in the Briançonnais Zone of the Cottian Alps. Specifically, the Mn-bearing minerals are hosted in Permian quartzites overlying quartzitic conglomerates (Verrucano formation) and quartz–feldspar fine-grained schists derived from Permian rhyolitic volcanism of the so-called Axial Permian–Carboniferous Zone (Franchi and Stella, 1930). A major subvertical tectonic contact, Faille de Ceillac (Gidon *et al.*, 1994), separates the rocks found at the Valletta mine from the Middle Triassic carbonate sequence of the Becco Grande to the north and from the Rocca La Meja ridge to the south. The rocks found at the Valletta mine are part of the Bande de Marinet, the southernmost tectonic zone of the Axial Permian–Carboniferous Zone; specifically, it is part of Unit M3, the structurally highest unit defined in the Bande de Marinet by Lefèvre (1982). During the Alpine tectonometamorphic cycle, the rocks now exposed in the Bande de Marinet were affected by high-*P*, low-*T* metamorphism of blueschist facies, the effects of which are more evident in the metabasites interlayered in the metavolcanic quartz–feldspar schists that often display the characteristic lawsonite–glaucophane assemblage (Franchi and Stella, 1930; Gidon *et al.*, 1994). Here, piccoliite is also always embedded in quartz matrix, associated with hematite, grandaite (Fig. 2b), tilasite/adelite, and, rarely, with thorianite. Other minerals that have been observed in the Valletta mine dump include aegirine, albite, aldomarinoite, azurite, baryte, bariopharmacosiderite, berzeliite, bosiite, braccoite, braunite, calcite, canosioite, castellaroite, coralloite, cryptomelane, diopside, fianelite, gamagarite, ganophyllite, gypsum, hollandite, ilmenite, lombardoite, magnesio-arfvedsonite, magnesio-riebeckite, magnetite, malachite, manganberzeliite, mimetite, muscovite (Mn-bearing), neotocite, opal, orthoclase, oxydravite (Fe^{3+}-Mn^{3+}-V^{3+}-rich), palenzonaite, phlogopite, pyrobelonite, ranciéite, rhodochrosite, rhodonite, richterite, rüdlingerite, rutile, saneroite, talc, tetrahedrite-series minerals, tinnunculite, tiragalloite, titanite, tokyoite, wallkilldellite, arsenate members of the alluaudite group, as well as other possible uncharacterised amphiboles (Cámara *et al.* 2022 and references therein). It is worth noting that many Mn-bearing phases at the Valletta mine contain iron exclusively as Fe^{3+} and manganese as Mn^{3+}.

Appearance and physical properties

Piccoliite occurs rarely at the Montaldo di Mondovì locality as black well-developed prismatic crystals within calcite–quartz veins (Fig. 2a), whereas it forms aggregates of anhedral crystals, embedded in the quartz matrix at the Valletta locality (Fig. 2b). Splinters may be very dark red. The streak is brown and the lustre is resinous to vitreous. The mineral is non-fluorescent and opaque, but transparent in thin section. Hardness was measured with Vickers indentation: four measurements were performed, with two different loads, obtaining VHN_{15} (two measurements) = 654 and 656 kg/mm^2 and VHN_{25} (two measurements) = 584 and 657 kg/mm^2, which corresponds to a Mohs hardness of 5–5½. Piccoliite is brittle, with no cleavage or parting observed. Fracture is irregular. Density was not measured because of the lack of heavy liquids of sufficient density. Calculated density is 4.084 g·cm^{-3} (based on the empirical formula and unit-cell volume refined from single-crystal X-ray diffraction data of the Montaldo di Mondovì specimen) and 4.011 g·cm^{-3} (Valletta sample).

Owing to the small amount of material available for the mineralogical study, the optical properties of piccoliite were determined in plane-polarised reflected light on a crystal fragment embedded in epoxy. Piccoliite is grey in colour. Under crossed polars, it is distinctly anisotropic, with rotation tints in shades of grey. Internal reflections in brownish tints are commonly observed. Reflectance was measured in air using a LEITZ microphotometer. Readings were taken for specimen and standard

https://doi.org/10.1180/mgm.2022.129 Published online by Cambridge University Press

(Zeiss SiC Standard 079) maintained under the same focus conditions for the standard wavelengths recommended by the Commission on Ore Mineralogy of the IMA. The edge of the square-like measuring area was ~0.1 mm. Reflectance values (R_{min}, R_{max} in %) for each λ (nm) are: 7.7, 9.8 at 470 nm; 7.7, 9.5 at 546 nm; 7.4, 9.3 at 589nm and 7.4, 9.2 at 650 nm.

The mean refractive index, calculated using the Gladstone–Dale relationship (Mandarino, 1979, 1981), and the calculated density of the Montaldo di Mondovì material, is 1.878.

Raman spectroscopy

Unpolarised micro-Raman spectra were obtained on an unpolished sample from the Montaldo di Mondovì locality in nearly back-scattered geometry with a Jobin-Yvon Horiba XploRA Plus apparatus, equipped with a motorised *x*–*y* stage and an Olympus BX41 microscope with a 10× objective. The 532 nm line of a solid-state laser was used. The minimum lateral and depth resolution was set to a few μm. The system was calibrated using the 520.6 cm^{-1} Raman band of silicon before each experimental session. Spectra were collected through multiple acquisition with single counting times of 180 s. Back-scattered radiation was analysed with a 1200 mm^{-1} grating monochromator. Peak deconvolution was performed through the software *Fityk* (Wojdyr, 2010).

In the range between 100 and 1200 cm^{-1} (Fig. 3a), the observed Raman spectrum in piccoliite from Montaldo di Mondovì is dominated by a band at ~850 cm^{-1}. Other bands are observed at (in cm^{-1}) 160, 191 (lattice vibrations), 342, 441, 488 (bending of As–O bonds), 745 (hydroxyl deformation band) and 803 (As–O stretching vibrations, along with the band at 894 cm^{-1}); band assignment is in agreement with Frost and Kloprogge (2003). The Raman spectrum of piccoliite from Valletta (Fig. 3a) shows the same bands at slightly different values due to the small difference in chemical composition (in cm^{-1}): 200, 318, 445, 518, 730, 800, 852 and 890. Differences in the intensity are probably due to the different crystallographic orientation of the grains studied.

In both spectra there are two bands at ~1650 and 1770 cm^{-1} that may correspond to overtones or combination modes of As–O-stretching vibrations, as no structural evidence in support of the presence of H_2O groups was found (see below).

Finally, in the (O–H)-stretching region (2800–3800 cm^{-1}), a broad band at 3140 cm^{-1} has been observed in the spectrum of piccoliite from Montaldo di Mondovì (Fig. 3b). The same spectral feature occurs in the spectrum collected on the sample from the Valletta mine but it shows a lower intensity. By using the relation of Libowitzky (1999), a donor–acceptor O···O distance of ~2.685 Å was calculated, in good agreement with the observed O7···O1 distance of 2.660(3) Å (see below). Similar bands are also found in the structurally related mineral carminite (Frost and Kloprogge, 2003).

Chemical composition

Preliminary energy dispersive spectroscopy analysis of piccoliite showed Na, Mg, Ca, Mn, Fe and As being the only elements present with atomic number > 8. Quantitative chemical analyses were carried out on the crystal used for the crystal-structure refinement using a CAMECA SX50 electron microprobe (wavelength dispersive spectroscopy mode, 15 kV, 15 nA and nominal beam diameter of 1 μm). The elements Al, S, K, Ti, Cr, Ni, Cu and Ba were sought but found to be below the detection limit. Counting times were 20 s on the peak and 10 s on the backgrounds for Na, and 30 s on the peak and 15 s on the background for all the other elements. Direct H_2O determination was not performed because of the very small amount of material available. Chemical data are given in Table 2.

The empirical formula of piccoliite, based on 10 (O,OH) anions per formula unit (pfu) and 6 cations pfu, is $(Na_{0.64}Ca_{0.35})_{\Sigma 0.99}$

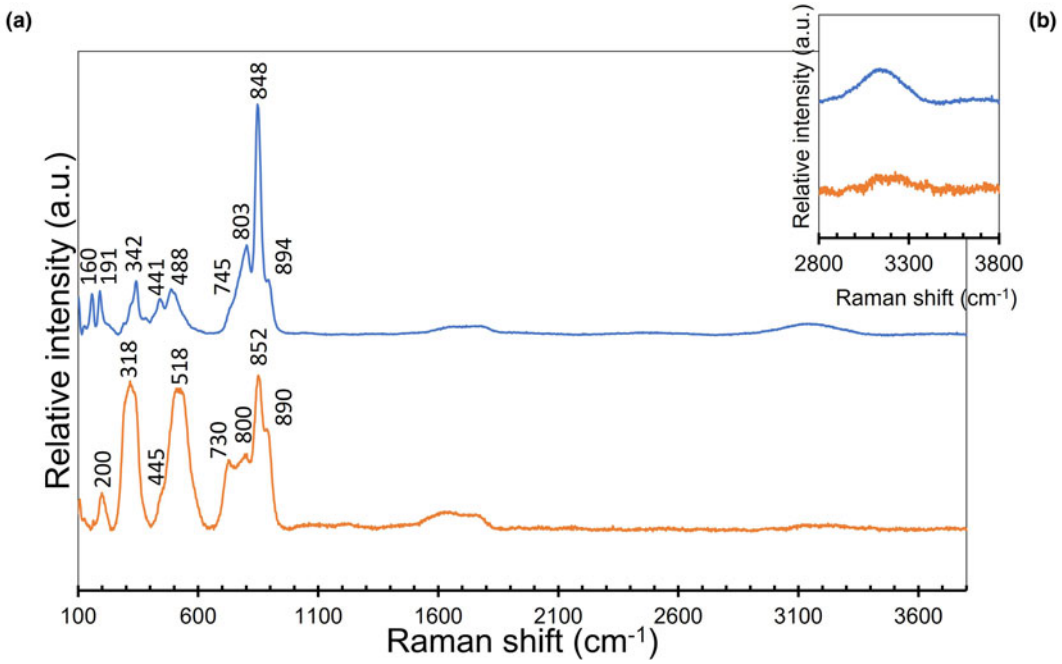

Fig. 3. Raman spectrum of piccoliite from Montaldo di Mondovì (upper, in blue) and from Valletta (lower, in orange) in the region 100–1200 cm^{-1} (a) and 2800–3800 cm^{-1} (b).

https://doi.org/10.1180/mgm.2022.129 Published online by Cambridge University Press

Table 2. Chemical data (in wt.%) for piccoliite

	Montaldo di Mondovì (n = 10)			Valletta (n = 13)			
Oxide	mean	range	s.u.	mean	range	s.u.	Probe standard
P_2O_5	0.06	0.00–0.14	0.04	0.08	0.03–0.14	0.04	apatite
V_2O_5	0.47	0.45–0.50	0.02	0.08	0.05–0.11	0.02	V_2O_3 (synthetic)
As_2O_5	48.06	47.21–48.90	0.53	47.90	46.91–48.72	0.51	GaAs (synthetic)
SiO_2	0.10	0.06–0.12	0.02	0.15	0.10–0.51	0.11	wollastonite
Mn_2O_3	17.48	17.07–18.00	0.30	16.20	15.35–16.80	0.43	rhodonite
MnO_2*				6.28			
Mn_2O_3*				10.50			
Fe_2O_3	9.74	9.11–10.24	0.34	8.32	7.17–9.33	0.90	magnetite
MgO	1.67	1.58–1.84	0.09	4.12	3.72–4.87	0.46	periclase
CaO	13.84	13.65–14.04	0.11	15.44	14.62–16.34	0.55	wollastonite
ZnO	–	–	–	0.07	0.00–0.15	0.05	Zn (synthetic)
SrO	–	–	–	0.13	0.06–0.28	0.06	celestine
Na_2O	5.54	5.21–5.75	0.16	5.01	4.65–5.32	0.21	jadeite
H_2O_{calc}**	1.86			1.90			
Total	98.82			99.98			

Note: s.u. = standard uncertainty; – = not detected
*The Mn^{4+}/Mn^{3+} ratio was calculated on the basis of 6 cations and 10 anions pfu; **H_2O was calculated on the basis of one OH group pfu.

$(Ca_{0.75}Na_{0.24})_{\Sigma 0.99}(Mn^{3+}_{1.08}Fe^{3+}_{0.59}Mg_{0.20}Ca_{0.10})_{\Sigma 1.97}(As_{2.03}V_{0.03}Si_{0.01})_{\Sigma 2.07}O_9(OH)$ for Montaldo di Mondovì and $(Na_{0.53}Ca_{0.47})_{\Sigma 1.00}(Ca_{0.76}Na_{0.23}Sr_{0.01})_{\Sigma 1.00}(Mn^{3+}_{0.63}Fe^{3+}_{0.49}Mg_{0.48}Mn^{4+}_{0.34}Ca_{0.06})_{\Sigma 2.00}(As_{1.97}P_{0.01}Si_{0.01})_{\Sigma 1.99}O_9(OH)$ for Valletta mine. All Fe is given as Fe^{3+}, whereas H_2O was calculated from stoichiometry to correspond to 1 (OH) pfu. See below for the discussion on oxidation state of Mn in the material studied from both localities. The ideal formula of piccoliite is $NaCaMn^{3+}_2(AsO_4)_2O(OH)$, corresponding to Na_2O 6.41, CaO 11.59, Mn_2O_3 32.63, As_2O_5 47.51, H_2O 1.86, total 100.00 wt.%.

X-ray crystallography

Powder X-ray diffraction data were collected on Montaldo di Mondovì material using a 114.6 mm Gandolfi camera. Data (in Å, for Cu$K\alpha$) are listed in Table 3. Unit-cell parameters were refined from the powder X-ray data using the method of Holland and Redfern (1997) based on 14 unequivocally indexed reflections. Refined unit-cell parameters are $a = 8.879(2)$, $b = 7.509(2)$, $c = 11.707(2)$ Å and $V = 779.7(2)$ Å^3 with $Z = 4$.

Single-crystal X-ray diffraction intensity data were collected on a $0.080 \times 0.040 \times 0.035$ mm crystal from Montaldo di Mondovì using a Bruker Smart Breeze diffractometer equipped with an air-cooled CCD detector, and graphite-monochromatised Mo$K\alpha$ radiation (Dipartimento di Scienze della Terra, Università di Pisa). The detector-to-crystal distance was 50 mm. Data were collected using ω and φ scans, in 0.5° slices, with an exposure time of 45 s per frame and corrected for Lorentz and polarisation factors and absorption using the software package *Apex2* (Bruker AXS Inc., 2004). Data were obtained on a $0.243 \times 0.194 \times 0.119$ mm crystal from Valletta mine using an Oxford Gemini R Ultra diffractometer equipped with a CCD area detector at CrisDi (Università di Torino), with graphite-monochromatised Mo$K\alpha$ radiation. The detector-to-crystal distance was 54.8 mm. Data were collected using ω scan modes, in 1° slices, with an exposure time of 17 s per frame and corrected for Lorentz and polarisation factors and absorption using the software package *CrysAlisPro* (Agilent Technologies, 2015).

Observed unit-cell parameters (Table 4) are consistent with orthorhombic symmetry. The statistical tests on the distribution

Table 3. Measured and calculated powder X-ray diffraction data for piccoliite from Montaldo di Mondovì.*

I_{obs}	d_{obs}	I_{calc}	d_{calc}	$h\ k\ l$
w	5.73	11	5.74	1 1 0
m	**4.85**	57	4.88	1 0 2
w	4.05	14	4.09	1 1 2
vw	3.805	6	3.822	2 1 0
w	3.607	14	3.633	2 1 1
		11	3.579	0 2 1
m	**3.470**	35	3.462	1 2 0
vs	**3.167**	59	3.223	1 1 3
		7	3.199	2 1 2
		100	3.162	0 2 2
w	2.932	20	2.922	0 0 4
w	2.786	16	2.786	2 2 1
m	**2.742**	30	2.753	3 1 0
		11	2.728	2 1 3
ms	**2.683**	14	2.705	0 2 3
		53	2.680	3 1 1
ms	**2.580**	37	2.604	1 1 4
		50	2.575	2 2 2
m	2.495	32	2.491	3 1 2
vw	2.442	14	2.441	2 0 4
m	**2.325**	19	2.325	3 2 0
		9	2.321	2 1 4
		9	2.310	2 2 3
w	2.239	5	2.249	3 1 3
w	2.171	9	2.165	1 1 5
w	2.000	5	1.994	2 1 5
w	1.888	5	1.886	4 2 1
		7	1.880	0 4 0
vw	1.814	5	1.818	3 3 2
vw	1.772	5	1.782	3 1 5
		12	1.767	4 0 4
m	1.732	24	1.731	2 4 0
		14	1.730	0 2 6
		19	1.717	3 3 3
vw	1.661	4	1.657	5 1 2
m	1.607	8	1.612	2 2 6
		27	1.600	3 3 4
m	1.584	18	1.581	0 4 4
		11	1.578	5 1 3

*Intensity and d_{hkl} (in Å) were calculated using the software *PowderCell 2.3* (Kraus and Nolze, 1996) on the basis of the structural model given in Table 5. The seven strongest reflections are given in bold. Intensities were visually estimated: vs = very strong; ms = medium–strong; m = medium; w = weak; and vw = very weak.

https://doi.org/10.1180/mgm.2022.129 Published online by Cambridge University Press

Table 4. Crystal and experimental data for piccoliite.*

	Montaldo di Mondovì	Valletta
Crystal data		
Crystal size (mm)	0.080 × 0.040 × 0.035	0.243 × 0.194 × 0.119
Cell setting, space group	Orthorhombic, *Pbcm*	Orthorhombic, *Pbcm*
a (Å)	8.8761(9)	8.8889(2)
b	7.5190(8)	7.5269(1)
c	11.6890(12)	11.6795(2)
V (Å^3)	780.12(12)	781.43(2)
Z	4	4
Data collection and refinement		
Radiation, wavelength (Å)	Mo*Kα*, 0.71073	Mo*Kα*, 0.71073
Temperature (K)	293	293
$2\theta_{max}$ (°)	72.10	91.33
Measured reflections	12281	66269
Unique reflections	1885	3442
Reflections with $F_o > 4\sigma(F_o)$	1554	3242
R_{int}	0.0256	0.0708
R_σ	0.0193	0.0208
Range of *h*, *k*, *l*	$-14 \le h \le 14$, $-12 \le k \le 12$, $-19 \le l \le 16$	$-17 \le h \le 17$, $-15 \le k \le 15$, $-23 \le l \le 23$
R_1 [$F_o > 4\sigma(F_o)$]	0.0250	0.0260
R_1 (all data)	0.0358	0.0288
wR_2 (on F_o^2)	0.0506	0.0576
Gof	1.115	1.289
Refined parameters	88	88
Maximum and minimum residual peak (e^- Å^{-3})	0.71 (at 0.54 Å from O1) −1.21 (at 1.29 Å from As1)	0.99 (at 0.57 Å from As1) −1.13 (at 0.21 Å from O1)

*Note: for the specimen from Montaldo di Mondovì, Kolitsch (2008) gives the following unit-cell parameters (space group *Pbcm*) from his preliminary crystal-structure determination [$R(F) = 0.0195$]: $a = 8.885(2)$, $b = 7.535(2)$, $c = 11.707(2)$ Å and $V = 783.8(3)$ Å^3. The weighting scheme is defined as follows: $w = q / [\sigma^2(F_o^2) + (a \times P)^2 + b \times P + d + e \times \sin(\theta)/\lambda]$ where $P = [0.33333 \times \text{Maximum of } (0 \text{ or } F_o^2) + (1–0.333333) \times F_c^2]$; used values are $a = 0.0210$ and $b = 0.5539$ for the Montaldo di Mondovì sample and $a = 0.0121$ and $b = 0.6188$ for the Valletta sample.

Table 5. Atomic sites, multiplicity (m) and Wyckoff letter (W), site occupancy (s.o.), atom fractional coordinates, and equivalent isotropic or isotropic (*) displacement parameters (in Å^2) for piccoliite.

Holotype (Montaldo di Mondovì)						
Site	mW	s.o.	*x/a*	*y/b*	*z/c*	$U_{eq/iso}$
*A*1	4*d*	$Na_{0.62(1)}Ca_{0.38(1)}$	0.92503(9)	0.99267(11)	¾	0.0154(3)
*A*2	4*c*	$Ca_{0.774(9)}Na_{0.226(9)}$	0.41855(7)	¾	½	0.0196(3)
Mn	8*e*	$Mn_{0.902(3)}Mg_{0.098(3)}$	0.25110(3)	0.38099(4)	0.11573(2)	0.00802(9)
*As*1	4*d*	$As_{1.00}$	0.42831(3)	0.01033(3)	¼	0.00734(6)
*As*2	4*c*	$As_{1.00}$	0.93470(3)	¼	0	0.00694(6)
O1	4*d*	$O_{1.00}$	0.3076(3)	0.8418(3)	¼	0.0306(6)
O2	8*e*	$O_{1.00}$	0.5352(2)	0.0020(2)	0.3699(1)	0.0136(3)
O3	4*d*	$O_{1.00}$	0.3207(2)	0.1989(2)	¼	0.0114(3)
O4	8*e*	$O_{1.00}$	0.8167(2)	0.0759(2)	0.0061(1)	0.0134(2)
O5	8*e*	$O_{1.00}$	0.0409(2)	0.2674(2)	0.1192(1)	0.0124(2)
O6	4*c*	$O_{1.00}$	0.3269(2)	¼	0	0.0086(3)
O7	4*d*	$O_{1.00}$	0.1870(2)	0.5178(2)	¼	0.0093(3)
H7	4*d*	$H_{1.00}$	0.228(5)	0.612(7)	¼	0.040(14)*
Co-type (Valletta)						
Site	mW	s.o.	*x/a*	*y/b*	*z/c*	$U_{eq/iso}$
*A*1	4*d*	$Na_{0.498(7)}Ca_{0.502(7)}$	0.92471(6)	0.99221(7)	¾	0.0127(2)
*A*2	4*c*	$Ca_{0.777(7)}Na_{0.223(7)}$	0.41861(5)	¾	½	0.0190(2)
Mn	8*e*	$Mn_{0.729(3)}Mg_{0.271(3)}$	0.25125(2)	0.38212(3)	0.11582(2)	0.00792(6)
*As*1	4*d*	$As_{1.00}$	0.42830(2)	0.01147(2)	¼	0.00703(3)
*As*2	4*c*	$As_{1.00}$	0.93401(2)	¼	0	0.00672(3)
O1	4*d*	$O_{1.00}$	0.3076(2)	0.8431(2)	¼	0.0296(5)
O2	8*e*	$O_{1.00}$	0.53472(11)	0.00294(14)	0.37002(8)	0.01284(16)
O3	4*d*	$O_{1.00}$	0.31970(16)	0.19908(18)	¼	0.0107(2)
O4	8*e*	$O_{1.00}$	0.81624(12)	0.07521(13)	0.00456(9)	0.01368(16)
O5	8*e*	$O_{1.00}$	0.04027(11)	0.26646(14)	0.11951(8)	0.01251(15)
O6	4*c*	$O_{1.00}$	0.32822(14)	¼	0	0.00862(17)
O7	4*d*	$O_{1.00}$	0.18558(16)	0.51972(18)	¼	0.0110(2)
H7	4*d*	$H_{1.00}$	0.220(5)	0.609(8)	¼	0.052(15)*

https://doi.org/10.1180/mgm.2022.129 Published online by Cambridge University Press

of $|E|$ values ($|E^2-1| = 0.872$) and the systematic absences suggested the space group symmetry *Pbcm*. The crystal from Valletta showed significant systematic absences violations of the *c*-glide but further examination of structural models having a lower symmetry led to models that were equivalent to a *Pbcm* structure. The violations of systematic absences may be due to double diffraction phenomena. The crystal structure was solved through direct methods using *SHELXS*-97 (Sheldrick, 2008). After locating the heavier atoms, the structure solution was completed through successive difference-Fourier syntheses and refined using *SHELXL*-2014 (Sheldrick, 2015). Scattering curves for neutral atoms were taken from the *International Tables for Crystallography* (Wilson, 1992). The following curves were used: Ca *vs.* Na at the *A*1 and *A*2 sites; Mn *vs.* Mg at the *Mn* site; As at the *As*1 and *As*2 sites; and O at the O1–O7 sites. The *As*1, *As*2 and O sites were found to be fully occupied by As and O, respectively. The *A*1 and *A*2 sites have a mixed (Na,Ca) and (Ca,Na) occupancy, respectively. Owing to the similar scattering factors of Mn and Fe, the occupancy of the *Mn* site was refined based on the chemical-analytical data: mixed (Mn,Fe) occupancy with minor Mg and Ca. The H atom bonded to the oxygen atom hosted at the O7 site was found in the difference-Fourier map. After several cycles of anisotropic refinement (only H was refined isotropically), the R_1 factor converged to 0.0250 for 1554 reflections with $F_o > 4\sigma(F_o)$ for the crystal from the Montaldo di Mondovì mine, and 0.0260 for 3242 reflections with $F_o > 4\sigma(F_o)$ for the crystal from the Valletta mine. Details of data collection and refinement are given in Table 4. Fractional atom coordinates, site occupancies and equivalent isotropic or isotropic displacement parameters are reported in Table 5. The crystallographic information file has been deposited with the Principal Editor of *Mineralogical Magazine* and is available as Supplementary material (see below). Table 6 reports selected bond distances. Table 7 shows the comparison between observed site scattering and that calculated from the proposed site population. Finally, Tables 8 and 9 provide a bond-valence analysis carried out using the bond-valence parameters of Gagné and Hawthorne (2015).

Table 6. Selected bond lengths (in Å) for piccoliite.

	Montaldo di Mondovì	Valletta
*A*1–O7	2.327(2)	2.321(2)
*A*1–O1	2.411(3)	2.409(2)
*A*1–O5 ×2	2.500(2)	2.492(1)
*A*1–O5 ×2	2.579(2)	2.584(1)
*A*1–O3	2.614(2)	2.606(2)
*A*1–O4	3.206(2)	3.187(1)
<*A*1–O>	2.658	2.651
*A*2–O6	2.259(2)	2.250(1)
*A*2–O2 ×2	2.441(2)	2.436(1)
*A*2–O4 ×2	2.465(2)	2.468(1)
*A*2–O2 ×2	2.641(2)	2.645(1)
*A*2–O1	3.160(1)	3.161(1)
<*A*2–O>	2.630	2.630
Mn–O6	1.804(1)	1.813(1)
Mn–O7	1.961(1)	1.967(1)
Mn–O4	2.038(1)	2.040(1)
Mn–O5	2.052(1)	2.068(1)
Mn–O2	2.111(1)	2.115(1)
Mn–O3	2.172(1)	2.174(1)
<*Mn*–O>	2.023	2.029
*D.I.**	0.04637	0.04578
*As*1–O1	1.660(2)	1.660(2)
*As*1–O2 ×2	1.694(1)	1.692(1)
*As*1–O3	1.710(2)	1.711(1)
<*As*1–O>	1.690	1.690
*D.I.**	0.00877	0.00843
*As*2–O4 ×2	1.678(1)	1.682(1)
*As*2–O5 ×2	1.688(1)	1.690(1)
<*As*2–O>	1.683	1.690
*D.I.**	0.00281	0.00232
O7···H7	0.80(6)	0.74(6)
O1···H7	1.87(6)	1.93(6)
O7···O1	2.661(3)	2.665(3)
O7–H7–O1	175(5)°	179(6)°

* *D.I.* = Distortion index of bond lengths (Baur, 1974)

X-ray absorption spectroscopy

X-ray absorption spectroscopy (XAS) measurements at the *K*-edge of Mn were performed at the LISA beamline (BM-08) (d'Acapito *et al.*, 2019) at the European Synchrotron Radiation Facility (ESRF), Grenoble, France. Samples were measured using a pair of Si (111) flat crystals; Si-coated focusing mirrors ($E_{cutoff} \approx 16$ KeV) were used for harmonic rejection. Measurements were performed on a single crystal in the fluorescence mode using a four-channel Silicon Drift Detector (SDD) ARDESIA (Hafizh *et al.*, 2019); Mn model compounds (rhodochrosite, bixbyite-(Mn) and pyrolusite) were measured in transmission mode. The spectra were acquired with a fixed *k* step of 0.05 Å^{-1} up to a maximum value of 12 Å^{-1}. Samples were measured at room temperature. Standard procedures (Lee *et al.*, 1981) were followed to extract the structural extended X-ray absorption fine structure (EXAFS) signal ($k \bullet \chi(k)$): pre-edge background removal, spline modelling of bare atomic background, edge step normalisation using a region far above the edge, and energy calibration using the software *ATHENA* (Ravel and Newville, 2005). Model atomic clusters centred on the absorber atom were obtained by *ATOMS* (Ravel, 2001), using atomic coordinates taken from the crystal-structure determination reported in this study; theoretical amplitude and phase functions were generated using the *FEFF8* code (Ankudinov *et al.*, 1998). EXAFS spectra were fitted through the *ARTEMIS* software (Ravel and Newville, 2005) in the Fourier-Transform (FT) space.

The XAS spectrum in the X-ray absorption near edge structure (XANES) region of piccoliite is in Fig. 4, together with those of rhodochrosite, bixbyite-(Mn), pyrolusite and hollandite. An accurate quantification of Mn valence state is rather difficult, especially without comparison with well-known model compounds belonging to the same structural family, as different octahedral arrangements and distortions, especially related to Jahn-Teller effects, may affect the pre-edge peak intensity and the overall XANES shape, i.e. the features commonly used to evaluate Mn valence (see Farges, 2005 and Manceau *et al.*, 2012 for a detailed discussion). It is, therefore, safer to limit the discussion to a purely qualitative assessment. The position of the main absorption edge of piccoliite (main inflection point at 6548.4 eV), although lying close to that of bixbyite-(Mn) (6547.4 eV), is shifted towards higher energy values, clearly indicating the presence of a moderate quantity of Mn^{4+}. As a comparison, the edge position of hollandite (6551.4 eV, data from Manceau *et al.*, 2012), where the average Mn valence is close to 4+, lies much closer to that of pyrolusite (6552.4 eV).

https://doi.org/10.1180/mgm.2022.129 Published online by Cambridge University Press

Table 7. Refined *vs.* calculated site-scattering values (electrons per formula unit) and site population for piccoliite.

Site	Refined site scattering	Proposed site population	Calculated site scattering	Calc.* <*M*–O>	Obs. <*M*–O>
Montaldo di Mondovì					
*A*1	14.42(14)	$Na_{0.64}Ca_{0.35}$	14.04		
*A*2	17.97(16)	$Ca_{0.75}Na_{0.24}$	17.64		
Mn	47.45(14)	$Mn^{3+}_{1.08}Fe^{3+}_{0.59}Mg_{0.20}Ca_{0.10}$	46.74	2.010	2.023
Valletta					
*A*1	15.52(11)	$Na_{0.53}Ca_{0.47}$	15.23		
*A*2	17.99(13)	$Ca_{0.76}Na_{0.23}Sr_{0.01}$	18.11		
Mn	42.95(13)	$Mn^{3+}_{0.63}Fe^{3+}_{0.49}Mg_{0.48}Mn^{4+}_{0.34}Ca_{0.06}$	43.95	2.024	2.029

* Calculated using ionic radii from Shannon (1976); a radius of O^{2-} was taken as 1.37 Å considering average coordination number of bonding oxygen atoms.

Table 8. Weighted bond-valences (vu) for piccoliite.*

Montaldo di Mondovì

Site	*A*1	*A*2	*Mn*	*As*1	*As*2	Σanions	$\Sigma anions_{corr}$
O1	0.22	$0.04^{\downarrow\times2}$		1.35		1.61	1.83
O2		$0.25^{\downarrow\times2}$, $0.15^{\downarrow\times2}$	0.34	$1.22^{\downarrow\times2}$		1.96	
O3	0.14		$^{2\times\rightarrow}0.28$	1.17		1.87	
O4	$0.03^{\downarrow\times2}$	$0.23^{\downarrow\times2}$	0.44		$1.28^{\downarrow\times2}$	1.98	
O5	$0.18^{\downarrow\times2}$, $0.15^{\downarrow\times2}$		0.42		$1.25^{\downarrow\times2}$	1.99	
O6		0.39	$^{2\times\rightarrow}0.98$			2.33	
O7	0.27		$^{2\times\rightarrow}0.57$			1.41	2.19
Σcations	1.33	1.71	3.03	4.96	5.06		
WAV	1.34	1.74	2.82	5.00	5.00		

Valletta

Site	*A*1	*A*2	*Mn*	*As*1	*As*2	Σanions	$\Sigma anions_{corr}$
O1	0.24	$0.04^{\downarrow\times2}$		1.34		1.63	1.84
O2		$0.25^{\downarrow\times2}$, $0.15^{\downarrow\times2}$	0.35	$1.23^{\downarrow\times2}$		1.98	
O3	0.15		$^{2\times\rightarrow}0.29$	1.17		1.90	
O4	$0.04^{\downarrow\times2}$	$0.23^{\downarrow\times2}$	0.44		$1.27^{\downarrow\times2}$	1.97	
O5	$0.20^{\downarrow\times2}$, $0.16^{\downarrow\times2}$		0.40		$1.24^{\downarrow\times2}$	1.99	
O6		0.39	$^{2\times\rightarrow}0.88$			2.15	
O7	0.29		$^{2\times\rightarrow}0.54$			1.38	2.20
Σcations	1.48	1.73	2.90	4.97	5.01		
WAV	1.47	1.77	2.90	5.00	5.00		

*Notes: Left and right superscripts indicate the number of equivalent bonds involving anions and cations, respectively. Bond valence at mixed-occupancy sites were weighted and their BVS (Σcations) compared with the weighted atomic valences (WAV) from the empirical formula. BVS of anions (Σanions) have been corrected considering hydrogen bonds.

The Mn *K*-edge EXAFS spectrum and Fourier transform of piccoliite are shown in Fig. 5a and b, respectively; results of the EXAFS multiparameter fit are reported in Table 10. Attempts to fit the first shell using an average Mn–O distance calculated

Table 9. Weighted bond-valences (vu) for pilawite-(Y) (data from Pieczka *et al.* 2015).*

Site	*Y*1	*Ca*2	*Al*1	*Al*2	*Si*1	*Si*2	Σanions	$\Sigma anions_{corr}$
O1		0.28, 0.24		0.48	0.98		1.98	
O2		0.27, 0.23	0.50		0.99		1.99	
O3	0.35		0.55		0.99		1.89	
O4	0.41			0.53	0.97		1.91	
O5		0.24	0.35	0.31		0.91	1.81	
O6	0.27	0.27				1.00	1.54	1.91
O7	0.42, 0.29		0.39			0.95	2.05	
O8	0.34, 0.19			0.37		0.97	1.87	
O9	0.62		0.74	0.77			2.13	
O10		0.37	0.57	0.58			1.52	2.16
Σcations	2.89	1.90	3.10	3.04	3.93	3.83		
WAV	3.00	1.99	3.00	3.00	4.00	4.00		

*Notes: Bond valence at mixed-occupancy sites were weighted and their BVS (Σcations) compared with the weighted atomic valences (WAV) from the empirical formula. BVS of anions (Σanions) have been corrected considering hydrogen bonds.

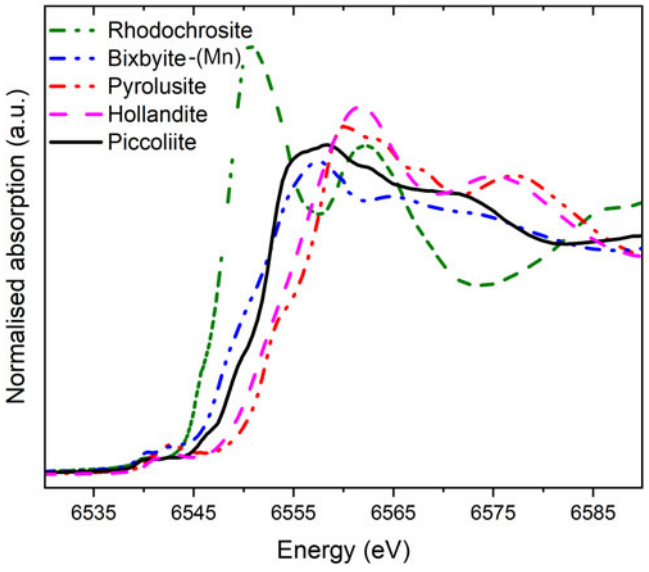

Fig. 4. Mn *K*-edge XANES of piccoliite from Valletta mine, together with rhodochrosite, bixbyite-(Mn), pyrolusite and hollandite (hollandite spectrum from Manceau *et al.*, 2012).

https://doi.org/10.1180/mgm.2022.129 Published online by Cambridge University Press

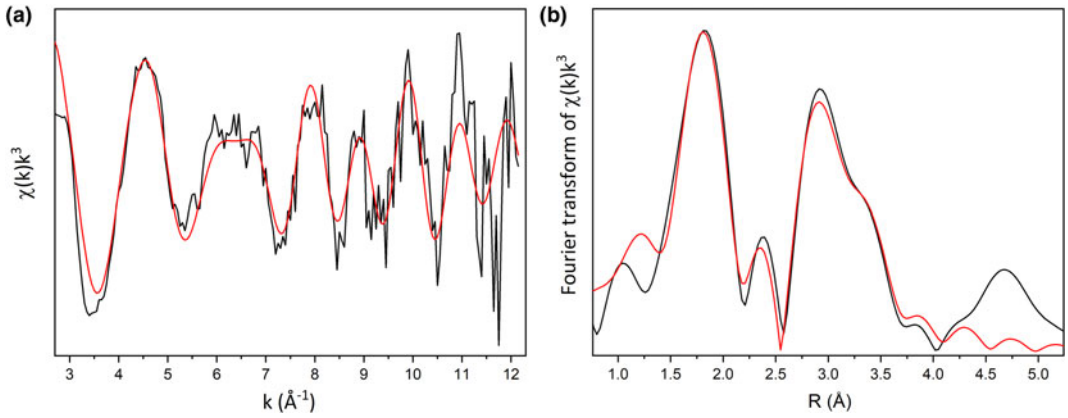

Fig. 5. Mn *K*-edge EXAFS (a) and Fourier transform, uncorrected for phase-shift (b) of piccoliite from Valletta mine.

from the starting model were unsuccessful, leading to a poor fit and an extremely high Debye–Waller factor (σ^2) [0.02(1) Å^{-2}]; only the use of six different Mn–O paths, as suggested by the crystal-structure data, gave a suitable fit for the data and resulted in a drop of σ^2 of a factor 5, thus confirming that Mn is hosted in a very distorted site. The set of six distances is in excellent agreement with the crystal-structure model (Table 6), resulting in a value of <Mn–O> = 2.03 Å. The second shell signal is dominated by the contribution of the four closest Mn–As scattering paths. Resulting Mn–As distances are in good agreement with those obtained by the crystal-structure refinement. Neither the contribution of the Mn–Mn/Mg scattering paths nor that of the Mn–Ca/Na ones was observable during the fit procedure. The lack of these contributions is probably due to destructive interferences occurring between the signals corresponding to the aforementioned paths as suggested in the Supplementary figure 1. It is noticeable, however, that Mn–As paths are not affected by this interference, and show higher amplitude at higher *k* values.

Structure description

The crystal structure of piccoliite (Fig. 6a) is characterised by $MnO_5(OH)$ octahedra forming edge-shared $[M\varphi_{10}]$ dimers; these dimers are connected through corner-sharing, forming two-up-two-down $[^{[6]}M_2(^{[4]}TO_4)_4\varphi_2]$ chains [M = Mn, T = As and φ = O(OH)] running along **c** (Fig. 6b, c). These chains are bonded in the **a** and **b** directions by sharing corners with AsO_4 tetrahedra, giving rise to a framework of tetrahedra and octahedra hosting Ca^{2+} and Na^{+} cations.

Arsenic is coordinated tetrahedrally by oxygen atoms, with <*As*–O> = 1.690 and 1.683 Å for the *As*1 and *As*2 sites, respectively (Montaldo di Mondovì data). The observed <*T*–O> value is in good agreement with the grand mean value reported for arsenates in the literature [1.687(27) Å, Gagné and Hawthorne, 2018]. The bond-valence sum (BVS) values at *As*1 and *As*2 are 4.96 and 5.06 valence units (vu), respectively. Trivalent Mn at the *Mn* site, partially replaced by Fe^{3+} and minor Mg^{2+}, and possibly Ca^{2+}, is hosted within a Jahn-Teller distorted octahedra, with bond distances ranging from 1.804(1) to 2.172(1) Å, and a <*Mn*–O> distance of 2.023 Å. Calculated BVS at the *Mn* site is 3.03 vu (Table 8), slightly larger than the expected atomic valence from site population (2.82 vu; Table 7). Finally, Ca and Na are hosted in the cavities of the octahedra and tetrahedra framework. Calcium is partitioned preferentially at the seven-fold coordinated *A*2 site, with average bond distance of 2.479 Å, whereas Na occurs at the seven-fold coordinated *A*1 site, having a slightly larger average bond distance (2.501 Å). The BVS at the *A*1 and *A*2 sites are 1.33 and 1.71 vu, respectively, in agreement with mixed (Na,Ca) and (Ca,Na) site populations, respectively (Table 8). The hydrogen atom is bonded to the oxygen hosted at the O7 site, forming a O7–H···O1 hydrogen bond. Its bond strength, calculated from the relation of Ferraris and Ivaldi (1988), is 0.25 vu.

The blackish colouration of the mineral suggests the presence of both Mn^{3+} and Mn^{4+} and XANES data indicate the presence of Mn^{4+} in piccoliite from the Valletta mine. Both mineralisations have a strongly oxidised character, with Fe always occurring as Fe^{3+} (e.g. hematite) and Mn as Mn^{3+} and Mn^{4+} (e.g. members of the hollandite supergroup). In agreement with this, the calculated bond valence incident at the *Mn* site for the Valletta specimen is larger than the expected from a formula without Mn^{4+} (2.89 vu *vs.* 2.73 vu, respectively), thus supporting a partial amount of more highly charged cations ordered at that site. The presence of Mn^{4+} is needed to charge balance the presence of Mg^{2+} at the *M* sites. It could be also balanced either by dehydroxylation at the O7 anion site or by an increase of Na (> 1 apfu) at the *A*1,2 sites. If we assume that part of the Mn is present as Mn^{4+} (likewise for the Montaldo di Mondovì sample), and we calculate 41% of Mn^{4+} in the bulk Mn, the average charge becomes +3.025, closer to the corresponding BVS calculated at the *M* sites (3.035 vu). Moreover, the calculated bond length would be 2.015 Å, closer to the observed value (2.023 Å) than

Table 10. Structural parameters from the Mn *K*-edge EXAFS analysis of piccoliite from Valletta mine.*

Shell	S_0^2	*R* (Å)	σ^2 (Å^{-2})
Mn–O		1.81(1)	0.006(2)
//		1.97(1)	//
//		2.04(1)	//
//		2.07(1)	//
//		2.13(1)	//
//	0.7 (1)	2.18(1)	//
Mn–As		3.27(1)	0.001(1)
//		3.38(1)	//
//		3.54(4)	0.012(5)
//		3.62(4)	//

*S_0^2 = Many-body amplitude reduction factor, *R*= interatomic distance, σ^2= Debye-Waller factor. Errors as reported in *ARTEMIS*.

https://doi.org/10.1180/mgm.2022.129 Published online by Cambridge University Press

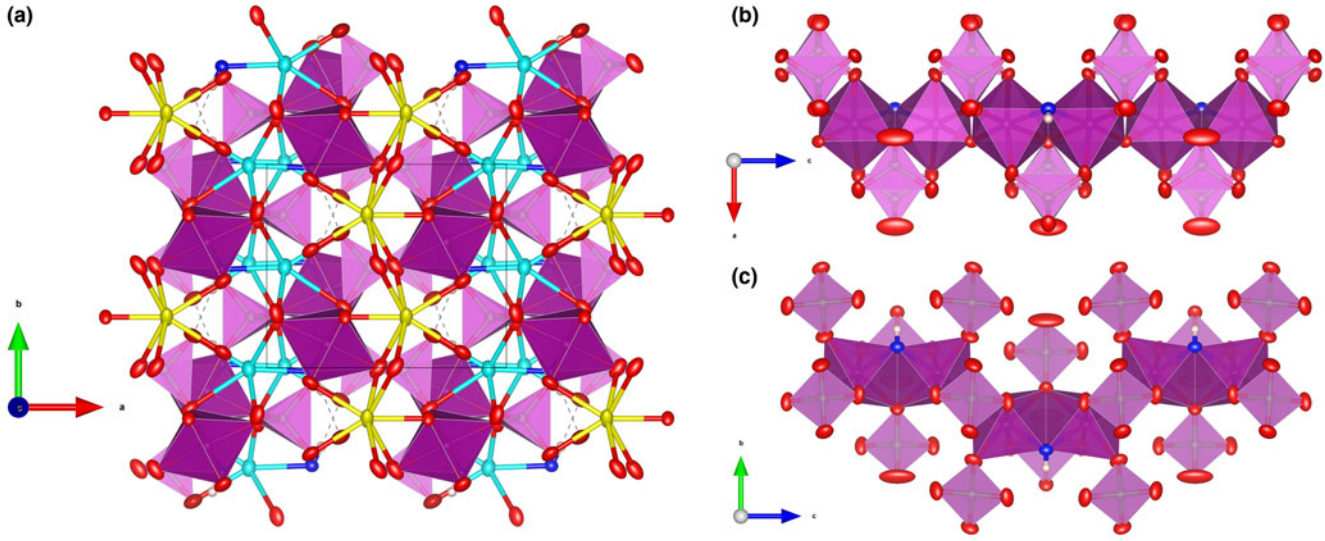

Fig. 6. Crystal structure of piccoliite, as seen down **c** (a). In (b) and (c), the chains of octahedra, decorated on both sides by (AsO_4) tetrahedra and running along **c**, are shown along **b** and **a**, respectively. Symbols: light pink polyhedra = *As*-centred tetrahedra; purple polyhedra = *Mn*-centred polyhedra; light blue ellipsoids = *A*1 site; yellow ellipsoids = *A*2 site; red ellipsoids = O1–O6 sites; blue ellipsoid: O7 site; white sphere: H7 site; dashed lines represent hydrogen bonds. Figure obtained with *Vesta 3* (Momma and Izumi, 2011).

the value calculated if all Mn is considered Mn^{3+} (2.041 Å). Besides, if all the Mn is considered as Mn^{3+} there is an O site with a relatively high BVS of ~2.33 vu (see Table 8). The assumed presence of 41% of Mn^{4+} would reduce the BVS to 2.24 vu, still high and thus showing a weakness for this topology. This remanent high BVS is due to the presence of a very short distance (*M*–O6 = 1.804 Å) compared to the average equatorial bond distance of the MO_6 octahedron (2.093 Å). This distance is even shorter than the one observed by Gagné and Hawthorne (2020) for both six-fold coordinated Mn^{3+} and Mn^{4+}, 1.843 and 1.841 Å, respectively. The BVS values reported in Table 8 for the crystal from Valletta when considering 35% of Mn^{4+} reduces the BVS at O6 to 2.145 vu, and yields a calculated averaged bond length of 2.024 Å, very close to the one observed (2.029 Å); moreover, the observed BVS at the *M* site (2.897 vu) is almost coincident with the average charge (+2.900). In any case, both XANES data and crystal-chemical considerations indicate that Mn in the Valletta specimen is mainly present at its trivalent state, thus Mn^{3+} is the dominant cation of the dominant charge (+3). The ideal-charge cation formula is thus $A1^{1+}\ A2^{2+}\ M^{3+}(T^{5+}O_4)O(OH)$.

The hydrogen-bonding topology is rather constrained and shows a O–H···O angle of 175(5)°. The donor–acceptor (O7···O1) distance is short (2.67 Å) but, using that donor–acceptor distance, the corresponding wavenumber value calculated using the relation of Libowitzky (1999), 3066 cm^{-1}, is in good agreement with the observed (OH)-stretching Raman shifts (3124 and 3252 cm^{-1}). The presence of two bands could agree with two local arrangements with two Mn^{3+} or one Mg^{2+} and Mn^{4+} in agreement with the proposed presence of Mn^{4+} at the *M* sites, as the O7 site is shared by two edge-sharing MO_6 octahedra. Further shifts can be attributed to the mixed valence at the *A*1 site, also coordinating the O7 anion site.

Relation to other species

The topology of the piccoliite structure is not new. The mineral pilawite-(Y), ideally $CaYAl_2(SiO_4)_2O(OH)$ (Pieczka *et al.*, 2015), has the same topology (see Fig. 7b), although its symmetry is monoclinic ($P2_1/c$), with a β angle of 90.61(4)°. Consequently, pilawite-(Y) has two symmetrically independent *M* sites and two anions split in two non-symmetrically equivalent positions (O1, O2 and O7, O8, corresponding, respectively, to O5 and O2 in the piccoliite structure).

A particularity of the structure of piccoliite is the high U_{eq} value observed in both crystals for the anion at the O1 site (Table 5), coordinating the $As1O_4$ tetrahedron, which receives further bonding from the H bonded to O7. The observed value is three times the mean value observed for the other anion sites. The anisotropic displacement values also show a dynamic disordering of this anion site along [001] in the (010) plane. This is a particularly striking feature considering the stressed nature of the topology of the hydrogen bond and could be related to a particular instability of the structure that could relax at lower temperatures, lowering the symmetry to monoclinic by a shear in the (010) plane. Interestingly, the U_{eq} value of the corresponding O6 site in the pilawite-(Y) structure is still 50% higher than the average anion-site value, but much lower, in agreement with a monoclinic relaxation of a possible high-*T* orthorhombic structure, as suggested by Pieczka *et al.* (2015). Likewise, no anion site has a BVS > 2.1 vu in pilawite-(Y) (see Table 9). Both facts, along with the possible charge partitioning of Mn at the *M* site, may explain the weak violations of the *c*-glide observed in piccoliite from the Valletta Mine.

Other minerals related to piccoliite are reported in Table 11. The structure of carminite, palermoite and attakolite are reported in Fig. 7c, d and e, respectively, for comparison. These structures are not topologically congruent, as the $[^{[6]}M_2(^{[4]}TO_4)_4\varphi_2]$ chains cross-link in different ways in the **a** direction (Pieczka *et al.*, 2015), or in the **b** direction for palermoite (different cell setting; see Table 11). There is also a relative ½ shift of the chains along the chain direction between palermoite (and attakolite) and carminite. Palermoite and attakolite keep the same topology; attakolite relaxes to monoclinic due to the presence of $HSiO_4$ groups that point to an empty site alternating with

https://doi.org/10.1180/mgm.2022.129 Published online by Cambridge University Press

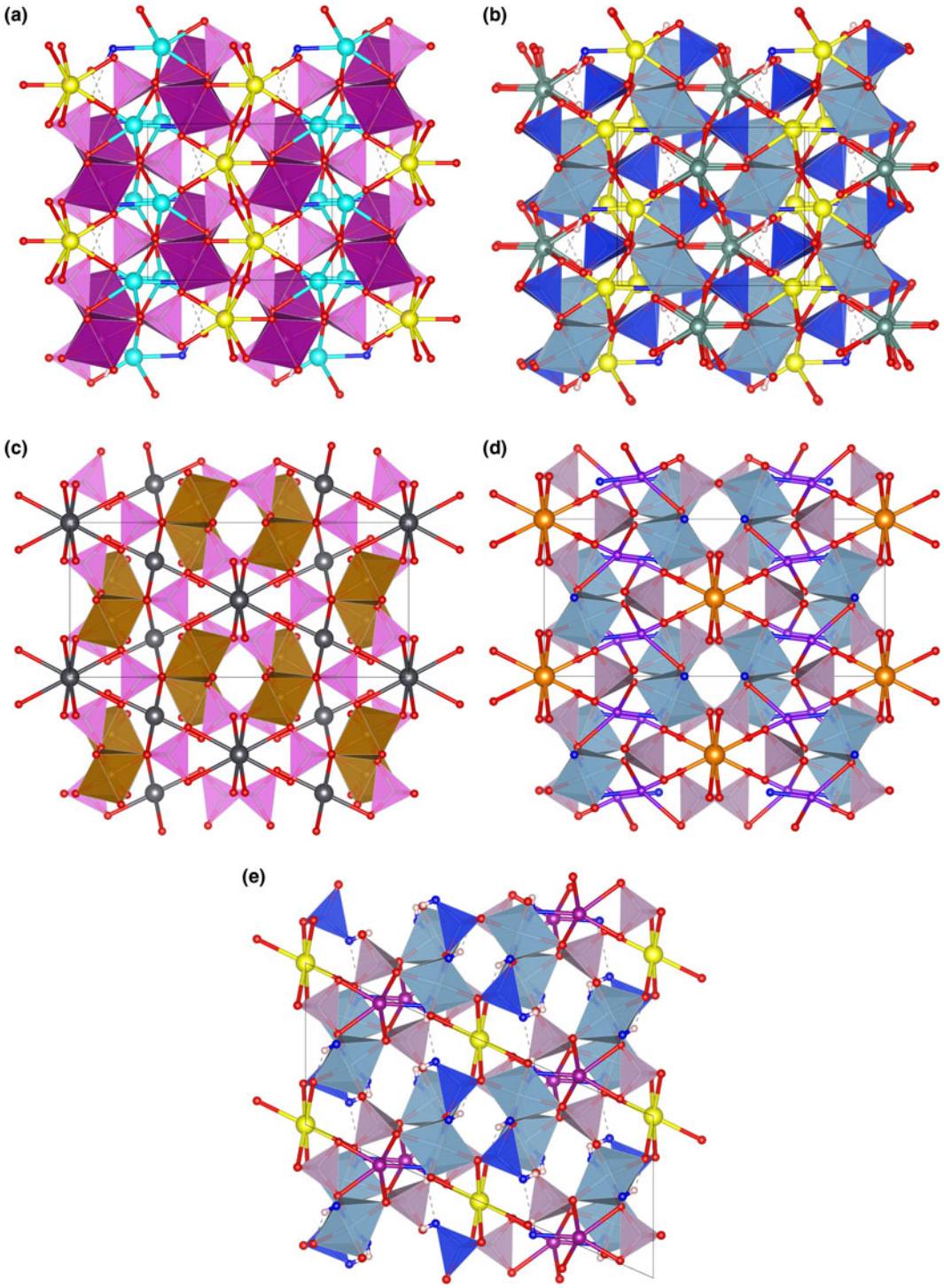

Fig. 7. The framework of octahedra and tetrahedra in piccoliite (a), pilawite-(Y) (b), carminite (c), palermoite (d) and attakolite (e), as seen along the chain direction. Seven-fold to eight-fold coordinated cations and their bonds are shown as ball-and-stick. Symbols: light pink polyhedra = *As*-centred tetrahedra; violet polyhedra = *P*-centred tetrahedra; blue polyhedra = *Si*-centred tetrahedra; purple polyhedra = *Mn*-centred polyhedra; cyan polyhedra = *Al*-centred octahedra; spheres: light blue = Na; yellow = Ca; red = O; purple = Mn; greyish blue = Y; dark grey = Pb; orange = Sr; violet = Li; blue = anion site hosting (OH) groups; white = H; dashed lines represent hydrogen bonds. Figure obtained with *Vesta 3* (Momma and Izumi, 2011).

Mn along [001]. This allows for the ordering of Si in 1 out of 4 sites with tetrahedral coordination, whereas high-charge cations (P in this case) order in tetrahedra without (OH) groups. Though these structures can be considered as having different polytypic stacking of the $[^{[6]}M_2(^{[4]}TO_4)_4\varphi_2]$ chains, the extra framework cavities are occupied by large cations (Sr, Pb, Y, Ca and Na) or smaller cations (Mn^{2+}, Li and H) with different bonding topologies, leading to different stoichiometries (from 4 to 3 apfu) and may not be strictly considered polytypes.

https://doi.org/10.1180/mgm.2022.129 Published online by Cambridge University Press

Table 11. Mineral species related to piccoliite.

Species	Chemical formula	*a* (Å)	*b* (Å)	*c* (Å)	β (°)	s.g.*	References
Piccoliite	$NaCaMn_2(AsO_4)_2O(OH)$	8.88	7.52	11.69		*Pbcm*	[1]
Pilawite-(Y)	$CaYAl_2(SiO_4)_2O(OH)$	8.56	7.26	11.18	90.6	$P2_1/c$	[2]
Carminite	$PbFe_2(AsO_4)_2(OH)_2$	16.59	7.58	12.28		*Cccm*	[3]
Crimsonite	$PbFe_2(PO_4)_2(OH)_2$	16.25	7.47	12.15		*Cccm*	[4]
Sewardite	$CaFe_2(AsO_4)_2(OH)_2$	16.46	7.43	12.13		*Cccm*	[5]
Attakolite	$CaMnAl_4[HSiO_4][PO_4]_3(OH)_4$	17.21	11.51	7.31	113.83	*C2/m*	[6]#
Bertossaite	$Ca_{0.5}LiAl_2(PO_4)_2(OH)_2$	11.48	15.73	7.23		*Imcb*	[7]
Palermoite	$Sr_{0.5}LiAl_2(PO_4)_2(OH)_2$	11.55	15.84	7.31		*Imcb*	[8]
Natropalermoite	$Sr_{0.5}NaAl_2(PO_4)_2(OH)_2$	11.48	16.25	7.29		*Imcb*	[9]

References: [1] this work; [2] Pieczka *et al.* (2015); [3] Kharisun *et al.* (1996); [4] Kampf *et al.* (2016); [5] Roberts *et al.* (2002); [6] Blomstrand (1868), redefined by Grice and Dunn (1992); [7] Hatert *et al.* (2011); [8] Moore and Araki (1975); [9] Schumer *et al.* (2017).
* s.g. = space-group type; # Mead and Mrose (1968) described a monoclinic cell *a* = 11.45, *b* = 15.69, *c* = 7.30 Å, β = 91.5° which resembles a relaxed cell of palermoite that would correspond to a *I*2/*m* s.g.

Acknowledgements. Reviewers Anthony R. Kampf, Adam Pieczka and Pete Leverett are thanked for useful suggestions. F.C. acknowledges financial support by the grant Ricerca Locale 2020, Università di Milano, and from the Italian Ministry of Education (MUR) through the project "Dipartimenti di Eccellenza 2018–2022". M.E.C. acknowledges financial support of AMI–Associazione Micromineralogica Italiana. Francesco d'Acapito and "LISA" CRG staff at ESRF (The European Synchrotron) are kindly acknowledged for the useful discussions and for the provision of in-house beamtime.

Supplementary material. To view supplementary material for this article, please visit https://doi.org/10.1180/mgm.2022.129

Competing interests. The authors declare none.

References

Agilent Technologies (2015) *CrysAlisPro software system, version 1.171.36.24*. Agilent Technologies UK Ltd., Oxford, UK.

Ankudinov A.L., Ravel B., Rehr J.J. and Conradson S.D. (1998) Real-space multiple-scattering calculation and interpretation of X-ray-absorption near-edge structure. *Physical Reviews,* **B58**, 7565–7576.

Basso R., Lucchetti G., Zefiro L. and Palenzona A. (1993) Mozartite, CaMn(OH)SiO_4, a new mineral species from the Cerchiara Mine, Northern Apennines, Italy. *The Canadian Mineralogist*, **31**, 331–336.

Basso R., Lucchetti G., Zefiro L. and Palenzona A. (2000) Cerchiaraite, a new natural Ba-Mn-mixed-anion silicate chloride from the Cerchiara mine, northern Apennines, Italy, *Neues Jahrbuch für Mineralogie, Monatshefte*, **2000**, 373–384.

Baur W.H. (1974) The geometry of polyhedral distortions. Predictive relationships for the phosphate group. *Acta Crystallographica,* **B30**, 1195–1215.

Biagioni C., Bonazzi P., Pasero M., Zaccarini F., Balestra C., Bracco R. and Ciriotti M.E. (2019) Manganiakasakaite-(La) and ferriakasakaite-(Ce), two new epidote supergroup minerals from Piedmont, Italy. *Minerals*, **9**, 353.

Blomstrand C.W. (1868) Om Westanå mineralier. *Öfversigt af Kongliga Vetenskaps- Akademiens Förhandlingar*, **25**, 197–212 [in Swedish].

Bonazzi P., Menchetti S. and Palenzona A. (1990) Strontiopiemontite, a new member of the epidote group, from Val Graveglia, Liguria, Italy. *European Journal of Mineralogy*, **2**, 519–523.

Bruker AXS Inc. (2004) *APEX* 2. Bruker Advanced X-ray Solutions, Madison, Wisconsin, USA.

Cabella R., Gaggero L. and Lucchetti G. (1992) Hollandite-cryptomelane and braunite in Mn-ores from upper Jurassic meta-arenites and marbles (Internal Brianconnais, Maritime Alps). *Atti dell'Accademia Nazionale dei Lincei. Rendiconti. Classe di Scienze fisiche, matematiche e naturali,* **3**, 33–41.

Cabella R., Lucchetti G. and Marescotti P. (1995) Sr-rich hollandite and cryptomelane in braunite-ores of Maritimes Alps and Eastern Liguria. *Neues Jahrbuch für Mineralogie, Monatshefte*, **1995**, 395–407.

Cabella R., Lucchetti G. and Marescotti P. (1999) Occurrence of LREE- and Y-arsenates from a Fe-Mn deposit, Ligurian Briançonnais Domain, Maritime Alps, Italy. *The Canadian Mineralogist*, **37**, 961–972.

Callegari A.M., Boiocchi M., Ciriotti M.E. and Balestra C. (2012) Coralloite, $Mn^{2+}Mn^{3+}_2(AsO_4)_2(OH)_2{\cdot}4H_2O$, a new mixed valence Mn hydrate arsenate: crystal structure and relationships with bermanite and whitmoreite mineral groups. *American Mineralogist*, **97**, 727–734.

Cámara F., Ciriotti M.E., Bittarello E., Nestola F., Massimi F., Radica F., Costa E., Benna P. and Piccoli G.C. (2014) As-bearing new mineral species from Valletta mine, Maira Valley, Piedmont, Italy. I. Grandaite, $Sr_2Al(AsO_4)_2(OH)$, description and crystal structure. *Mineralogical Magazine*, **78**, 757–774.

Cámara F., Biagioni C., Ciriotti M.E., Bosi F., Kolitsch U., Paar W.H., Blass G. and Bittarello E. (2017) Piccoliite, IMA2017-016. CNMNC Newsletter No. 37, June 2017, page 741. *Mineralogical Magazine*, **81**, 737–742.

Cámara F., Ciriotti M.E., Kolitsch U., Bosi F., Bittarello E., Brizio P., Vignola P. and Blaß G. (2021a) Armellinoite-(Ce), $Ca_4Ce^{4+}(AsO_4)_4{\cdot}H_2O$, a new mineral species isostructural with pottsite, $(Pb_3Bi)Bi(VO_4)_4{\cdot}H_2O$. *Mineralogical Magazine*, **85**, 901–909.

Cámara F., Kampf A.R., Nestola F., Ciriotti M.E., Spartà D. and Balestra C. (2021b) Demagistrisite, the missing link in a polysomatic series from lawsonite to orientite. *The Canadian Mineralogist*, **59**, 91–105.

Cámara F., Baratelli L., Ciriotti, M.E., Nestola F., Piccoli G.C., Bosi F., Bittarello, E., Hålenius U. and Balestra C. (2022) As-bearing new mineral species from Valletta mine, Maira Valley, Piedmont, Italy: IV. Lombardoite, $Ba_2Mn^{3+}(AsO_4)_2(OH)$ and aldomarinoite, $Sr_2Mn^{3+}(AsO_4)_2(OH)$, description and crystal structure. *Mineralogical Magazine*, **86**, 447–458.

Cenki-Tok B., Ragu A., Armbruster T., Chopin C. and Medenbach O. (2006) New Mn- and rare-earth-rich epidote-group minerals in metacherts: manganiandrosite-(Ce) and vanadoandrosite-(Ce). *European Journal of Mineralogy*, **18**, 569–582.

Ciriotti M.E. (2007) UM (Unnamed Minerals): i validi minerali senza nome del Piemonte e della Valle d'Aosta. Pp. 513–516 in: *Minerali del Piemonte e della Valle d'Aosta*. Associazione Amici del Museo "F. Eusebio", Alba, Cuneo, Italy, 607 pp. [in Italian].

Conti M. (1873) *Miniera di Ferro Ossidulato Manganesifero di Montaldo di Mondovì: Relazione Tecnica Sull'esercizio del Secondo Semestre 1872*. Tipografia Botta, Torino, Italy, 14 pp. [in Italian].

d'Acapito F., Lepore G.O., Puri A., Laloni A., La Mannna F., Dettona E., De Luisa A. and Martin A. (2019) The LISA beamline at ESRF. *Journal of Synchrotron Radiation*, **26**, 551–558.

Farges, F. (2005). Ab initio and experimental pre-edge investigations of the Mn K-edge XANES in oxide-type materials. *Physical Review B*, **71**, 155109.

Ferraris G. and Ivaldi G. (1988) Bond valence vs bond length in O···O hydrogen bonds. *Acta Crystallographica,* **B44**, 341–344.

Franchi S. and Stella A. (1930) *Carta Geologica d'Italia 1:100.000: Foglio 78–79 (Argentera-Dronero). 1ª edizione*. Regio Ufficio Geologico, Stabilimento Tipografico L. Salomone, Rome [in Italian].

Frost R.L. and Kloprogge J.T. (2003) Raman spectroscopy of some complex arsenate minerals – implications for soil remediation. *Spectrochimica Acta,* **A59**, 2797–2804.

Gagné O.C. and Hawthorne F.C. (2015) Comprehensive derivation of bond valence parameters for ion pairs involving oxygen. *Acta Crystallographica,* **B71**, 562–578.

Gagné O.C. and Hawthorne F.C. (2018) Bond-length distributions for ions bonded to oxygen: metalloids and post-transition metals. *Acta Crystallographica*, **B74**, 63–78.

Gagné O.C. and Hawthorne F.C. (2020) Bond-length distributions for ions bonded to oxygen: results for the transition metals and quantification of the factors underlying bond-length variation in inorganic solids. *IUCrJ*, **7**, 581–629.

Giai M. (2020) *Caratterizzazione Mineralogica della Miniera di Fe-Mn di Montaldo, Val Corsaglia, (Montaldo di Mondovì, Cuneo, Alpi Liguri)*. Master Thesis, Università di Torino, Italy, 147 pp. [in Italian].

Gidon M., Kerchove C., Michard A., Tricart P. and Goffé B. (1994) *Carte Géologique de la France à 1:50.000. Feuille Aiguille de Chambeyron (872). Notice Explicative*. BRGM, Service Géologique National, Orléans, France [in French].

Dalla Giovanna G. and Vanossi M. (1991) Le Unità piemontesi e brianzonesi tra le valli del Vermegnana e del Casotto. Pp. 163–185 in: *Guide Geologiche Regionali, Alpi Liguri*. Società Geologica Italiana, BE-Ma Editrice, Roma [in Italian].

Grice J.D. and Dunn P.J. (1992) Attakolite: New data and crystal-structure determination. *American Mineralogist*, **77**, 1285–1291.

Hafizh I., Bellotti G., Carminati M., Utica G., Gugiatti M., Balerna A., Tullio V., Lepore G.O., Borghi G., Ficorella F., Picciotto A., Zorzi N., Capsoni A., Coelli S., Bombelli L. and Fiorini C. (2019) Characterization of ARDESIA: a 4-channel SDD X-ray spectrometer for synchrotron measurements at high count rates. *Journal of Instrumentation*, **14**, P06027.

Haidinger W. (1828) Mineralogische Beschreibung der Manganerze IV. Brachytypes Manganerz, Braunit. *Annalen der Physik und Chemie*, **14**, 197–211 [in German].

Hatert F., Lefèvre P. and Fransolet A.-M. (2011) The crystal structure of bertossaite, $CaLi_2[Al_4(PO_4)_4(OH,F)_4]$. *The Canadian Mineralogist*, **49**, 1079–1087.

Holland T.J.B. and Redfern S.A.T. (1997) Unit cell refinement from powder diffraction data: the use of regression diagnostics. *Mineralogical Magazine*, **61**, 65–77.

Kampf A.R., Adams P.M., Mills S.J. and Nash B.P. (2016) Crimsonite, $PbFe_2^{3+}(PO_4)_2(OH)_2$, the phosphate analogue of carminite from the Silver Coin mine, Valmy, Nevada, USA. *Mineralogical Magazine*, **80**, 925–935.

Kampf A.R., Carbone C., Belmonte D., Nash B.P., Chiappino L. and Castellaro F. (2017) Alpeite, $Ca_4Mn_2^{3+}Al_2(Mn^{3+}Mg)(SiO_4)_2(Si_3O_{10})(V^{5+}O_4)(OH)_6$, a new ardennite-group mineral from Italy. *European Journal of Mineralogy*, **29**, 907–914.

Kenngott A. (1853) *Piemontit*. Pp. 74–75 in: *Das Mohs'sche Mineralsystem*. Verlag und Druck, Wien, Austria [in German]

Kharisun, Taylor M.R., Bevan D.J.M. and Pring A. (1996) The crystal structure of carminite: refinement and bond valence calculations. *Mineralogical Magazine*, **60**, 805–811.

Kolitsch U. (2008) The crystal structure of a new Ca-Na-Mn^{3+}-arsenate from a small metamorphic Mn deposit in Italy. *Geochimica and Cosmochimica Acta*, **72**, Special Supplement 12S, A487 [abstract].

Kolitsch U., Ciriotti M.E., Cadoni M., Armellino G., Piccoli G.C., Ambrino P., Blass G., Odicino G. and Ciuffardi M. (2011) Montaldo di Mondovì. Minerali della miniera di manganese e ferro. *Micro*, **9**, 4–21 [in Italian].

Kraus W. and Nolze G. (1996) POWDER CELL – a program for the representation and manipulation of crystal structures and calculation of the resulting X-ray powder patterns. *Journal of Applied Crystallography*, **29**, 301–303.

Lee P.A., Citrin P.H., Eisenberger P.T. and Kincaid B.M. (1981) Extended X-ray absorption fine structure – its strengths and limitations as a structural tool. *Reviews of Modern Physics*, **53**, 769–806.

Lefèvre R. (1982) *Les Nappes Briançonnaises Internes et Ultra-Briançonnaises Dans Les Alpes Cottiennes Méridionales*. Thèse Scientifique, Université Paris Sud - Paris XI, Orsay, France [in French].

Lepore G.O., Bindi L., Benedetto F.D., Mugnaioli E., Viti C., Zanetti A., Ciriotti M.E. and Bonazzi P. (2017) A multimethodic approach for the characterization of manganiceladonite, a new member of the celadonite family from Cerchiara mine, Eastern Liguria, Italy. *Mineralogical Magazine*, **81**, 167–173.

Libowitzky E. (1999) Correlation of O–H stretching frequencies and O–H···O hydrogen bond lengths in minerals. *Monatshefte für Chemie*, **130**, 1047–1059.

Maletto G. and Piccoli G.C. (2014) *Minerali in Val d'Ala*. Amici del Museo "F. Eusebio", Alba, Cuneo, Italy, 223 pp. [in Italian].

Manceau A., Marcus M. A. and Grangeon S. (2012). Determination of Mn valence states in mixed-valent manganates by XANES spectroscopy. *American Mineralogist*, **97**, 816–827.

Mandarino J.A. (1979) The Gladstone-Dale relationship. Part III. Some general applications. *The Canadian Mineralogist*, **17**, 71–76.

Mandarino J.A. (1981) The Gladstone-Dale relationship. Part IV. The compatibility concept and its application. *The Canadian Mineralogist*, **19**, 441–450.

Mead C.W. and Mrose M.E. (1968) Solving problems in phosphate mineralogy with the electron probe. *U.S. Geological Survey Professional Paper*, **600-D**, D204–D206.

Meisser N., Perseil E.A., Brugger J. and Chiappero P.J. (1999) Strontiomelane, $Sr(Mn^{4+}_6Mn^{3+}_2)O_{16}$, a new mineral species of the cryptomelane group from St. Marcel-Praborna, Aosta valley, Italy. *The Canadian Mineralogist*, **37**, 673–678.

Momma K. and Izumi F. (2011) VESTA 3 for three-dimensional visualization of crystal, volumetric and morphology data. *Journal of Applied Crystallography*, **44**, 1272–1276.

Moore P.B. and Araki T. (1975) Palermoite, $SrLi_2[Al_4(OH)_4(PO_4)_4]$: its atomic arrangement and relationship to carminite, $Pb_2[Fe_4(OH)_4(AsO_4)_4]$. *American Mineralogist*, **60**, 460–465.

Orlandi P., Pasero M., Rotiroti N., Olmi F., Demartin F. and Moëlo Y. (2004) Gramaccioliite-(Y), a new mineral of the crichtonite group from Stura Valley, Piedmont, Italy. *European Journal of Mineralogy*, **16**, 171–175.

Orlandi P., Biagioni C., Pasero M. and Mellini M. (2013) Lavoisierite, $Mn_8^{2+}[Al_{10}(Mn^{3+}Mg)][Si_{11}P]O_{44}(OH)_{12}$, a new mineral from Piedmont, Italy: the link between "ardennite" and sursassite. *Physics and Chemistry of Minerals*, **40**, 239–249.

Piccoli G.C. (2002) *Minerali delle Alpi Marittime e Cozie Provincia di Cuneo*. Associazione Amici del Museo "F. Eusebio", Alba, Cuneo, Italy, 366 pp. [in Italian].

Piccoli G.C. (2007) Giacimenti manganesiferi del Cuneese. Pp. 216–219 in: *Minerali del Piemonte e della Valle d'Aosta*. Associazione Amici del Museo "F. Eusebio", Alba, Cuneo, Italy, 607 pp. [in Italian].

Piccoli G.C., Kolitsch U., Blaß G. and Ciriotti M.E. (2007a) Berzeliite di Montaldo di Mondovì: prima segnalazione italiana. *Micro*, **5**, 49–54 [in Italian with abstract in English, French and German].

Piccoli G.C., Maletto G., Bosio P. and Lombardo B. (2007b) *Minerali del Piemonte e della Valle d'Aosta*. Associazione Amici del Museo "F. Eusebio", Alba, Cuneo, Italy, 607 pp. [in Italian].

Pieczka A., Hawthorne F.C., Cooper M.A., Szełęg E., Szuszkiewicz A., Turniak K, Nejbert K. and Ilnicki S. (2015) Pilawite-(Y), $Ca_2(Y,Yb)_2[Al_4(SiO_4)_4O_2(OH)_2]$, a new mineral from the Piława Górna granitic pegmatite, southwestern Poland: mineralogical data, crystal structure and association. *Mineralogical Magazine*, **79**, 1143–1157.

Ravel B. (2001) ATOMS: crystallography for the X-ray absorption spectroscopist. *Journal of Synchrotron Radiation*, **8**, 314–316.

Ravel B. and Newville M. (2005) ATHENA, ARTEMIS, HEPHAESTUS: data analysis for X-ray absorption spectroscopy using IFEFFIT. *Journal of Synchrotron Radiation*, **12**, 537–541.

Roberts A.C., Cooper M.A., Hawthorne F.C., Criddle A.J. and Stirling J.A.R. (2002) Sewardite, $CaFe_2^{3+}(AsO_4)_2(OH)_2$, the Ca-analogue of carminite, from Tsumeb, Namibia: description and crystal structure. *The Canadian Mineralogist*, **40**, 1191–1198.

Schumer B.N., Yang H. and Downs R.T. (2017) Natropalermoite, $Na_2SrAl_4(PO_4)_4(OH)_4$, a new mineral isostructural with palermoite, from the Palermo No. 1 mine, Groton, New Hampshire, USA. *Mineralogical Magazine*, **81**, 833–840.

Shannon R.D. (1976) Revised effective ionic radii and systematic studies of interatomic distances in halides and chalcogenides. *Acta Crystallographica,* **A32**, 751–767.

Sheldrick G.M. (2008) A short history of SHELX. *Acta Crystallographica*, **A64**, 112–122.

Sheldrick G.M. (2015) Crystal structure refinement with SHELXL. *Acta Crystallographica,* **C71**, 3–8.

https://doi.org/10.1180/mgm.2022.129 Published online by Cambridge University Press

Sismonda A. (1841a) Memoria sui terreni stratificati delle Alpi. *Memorie della Reale Accademia delle Scienze di Torino*, serie II, **3**, 53 pp. [in Italian].

Sismonda A. (1841b) Osservazioni geologiche sulla Alpi Marittime e Appennini Liguri. *Memorie della Reale Accademia delle Scienze di Torino*, serie II, **4**, 54 pp. [in Italian].

Vanossi M. (1980) Les unités géologiques des Alpes Maritimes entre l'Ellero et la mer Ligure: un aperçu schématique. *Memorie di Scienze Geologiche*, **34**, 101–142 [in French].

Vanossi M., Cortesogno L., Galbiati B., Messiga B., Piccardo G.B. and Vannucci R. (1986) Geologia delle Alpi Liguri, dati, problemi, ipotesi. *Memorie della Società Geologica Italiana*, **28**, 5–75 [in Italian].

Wilson A.J.C. (editor) (1992) *International Tables for Crystallography Volume C: Mathematical, Physical and Chemical Tables*. Kluwer Academic Publishers, Dordrecht, The Netherlands.

Wojdyr M. (2010) Fityk: a general-purpose peak fitting program. *Journal of Applied Crystallography*, **43**, 1126–1128.

https://doi.org/10.1180/mgm.2022.129 Published online by Cambridge University Press